









# Mitochondrial ferredoxin-like is essential for forming complex I-containing supercomplexes in Arabidopsis

Helene Röhricht <sup>1,†</sup> Jonathan Przybyla-Toscano,<sup>2,3,†,‡</sup> Joachim Forner <sup>4</sup> Clément Boussardon <sup>3</sup>  
Olivier Keech <sup>3</sup> Nicolas Rouhier <sup>2</sup> and Etienne H. Meyer <sup>1,\*</sup>

- 1 Department of Plant Physiology, Institute of Biology, Martin-Luther-University Halle-Wittenberg, D-06120 Halle (Saale), Germany
  - 2 Institut National de Recherche pour l'Agriculture, l'Alimentation et l'Environnement (INRAE), Interactions Arbres-Microorganismes (IAM), Université de Lorraine, F-54000 Nancy, France
  - 3 Department of Plant Physiology, Umeå Plant Science Centre, Umeå University, S-90187 Umeå, Sweden
  - 4 Department of Organelle Biology, Biotechnology and Molecular Ecophysiology, Max-Planck-Institute of Molecular Plant Physiology, D-14476 Potsdam-Golm, Germany
- † Present address: Laboratoire Physiologie Cellulaire & Végétale, Institut de Recherche Interdisciplinaire de Grenoble, Université Grenoble Alpes, Institut National de Recherche pour l'Agriculture, l'Alimentation et l'Environnement, Commissariat à l'Energie Atomique et aux Energie Alternatives, Centre National de la Recherche Scientifique, F-38000 Grenoble, France

\*Author for correspondence: etienne.meyer@pflanzenphys.uni-halle.de (E. H. M.)

†These authors contributed equally to this work.

The author responsible for distribution of materials integral to the findings presented in this article in accordance with the policy described in the Instructions for Authors (<https://academic.oup.com/plphys/pages/General-Instructions>) is Etienne H. Meyer.

Project design: O.K., N.R., E.H.M; experimental work: H.R., J.P.T., J.F., C.B., N.R., E.H.M; data analysis: H.R., J.P.T., O.K., N.R., E.H.M; paper writing: E.H.M. with contributions from all authors.

## Abstract

In eukaryotes, mitochondrial ATP is mainly produced by the oxidative phosphorylation (OXPHOS) system, which is composed of 5 multiprotein complexes (complexes I–V). Analyses of the OXPHOS system by native gel electrophoresis have revealed an organization of OXPHOS complexes into supercomplexes, but their roles and assembly pathways remain unclear. In this study, we characterized an atypical mitochondrial ferredoxin (mitochondrial ferredoxin-like, mFDX-like). This protein was previously found to be part of the bridge domain linking the matrix and membrane arms of the complex I. Phylogenetic analysis suggested that the *Arabidopsis* (*Arabidopsis thaliana*) mFDX-like evolved from classical mitochondrial ferredoxins (mFDXs) but lost one of the cysteines required for the coordination of the iron-sulfur (Fe-S) cluster, supposedly essential for the electron transfer function of FDXs. Accordingly, our biochemical study showed that AtmFDX-like does not bind an Fe-S cluster and is therefore unlikely to be involved in electron transfer reactions. To study the function of mFDX-like, we created deletion lines in *Arabidopsis* using a CRISPR/Cas9-based strategy. These lines did not show any abnormal phenotype under standard growth conditions. However, the characterization of the OXPHOS system demonstrated that mFDX-like is important for the assembly of complex I and essential for the formation of complex I-containing supercomplexes. We propose that mFDX-like and the bridge domain are required for the correct conformation of the membrane arm of complex I that is essential for the association of complex I with complex III<sub>2</sub> to form supercomplexes.

## Introduction

Respiration is a metabolic pathway essential for plant growth as it produces energy, in the form of ATP, required to sustain metabolism (Nicholls and Ferguson, 2013). Respiratory ATP is mainly produced in mitochondria by the ATP synthase located in the inner mitochondrial membrane (IMM). To convert ADP into ATP, the ATP synthase utilizes the electrochemical gradient built across the IMM by the respiratory chain. The respiratory chain recycles cofactors for upstream metabolic reactions and transfers protons from the matrix to the intermembrane space. Together the respiratory chain and the ATP synthase form the oxidative phosphorylation (OXPHOS) system. The plant OXPHOS system comprises 5 protein complexes (named complex I to V, complex V being the ATP synthase) and several individual proteins as well as a mobile electron carrier coenzyme Q (Braun, 2020).

The biochemical analysis of OXPHOS complexes may be carried out by native gel electrophoresis. After isolating mitochondria, protein complexes are solubilized using mild detergents and separated on a native gel (Schagger and von Jagow, 1991). Using very mild detergents such as digitonin or Triton X-100, additional bands, larger than the individual complexes, were observed and further analyses determined that these bands correspond to assemblies of OXPHOS complexes (Schagger and Pfeiffer, 2001). These stoichiometric arrangements of OXPHOS complexes are called supercomplexes. Such assemblies correspond to homodimers (complex V dimers), heterodimers (supercomplexes I + III<sub>2</sub> or III<sub>2</sub> + IV), or larger combinations (e.g. supercomplex I + III<sub>2</sub> + IV) (Lenaz and Genova, 2009; Enriquez, 2016). Supercomplexes were observed in all organisms investigated so far. However, the roles of these arrangements remain unresolved (Milenkovic et al., 2017; Hirst, 2018; Stuchebrukhov et al., 2020; Wu et al., 2020; Javadov et al., 2021).

Complex I is the largest OXPHOS complex (Hirst, 2013). In plants, it is composed of at least 47 subunits, of which nine subunits are encoded by genes present in the mitochondrial genome (Peters et al., 2013; Braun et al., 2014). Complex I is composed of 2 arms, the membrane arm embedded in the IMM, and the matrix arm that is attached at one end of the membrane arm. Each arm is composed of 2 modules. The matrix arm is formed by the N module where NADH binds and the Q module where ubiquinone is reduced. The membrane arm is divided into the so-called proximal (P<sub>p</sub>) module, where the matrix arm is bound and the distal (P<sub>d</sub>) module forming the tip of the membrane arm (Efremov and Sazanov, 2012; Letts and Sazanov, 2015). In plants, additional structures are present on the matrix side of the membrane arm: a globular structure formed by gamma carbonic anhydrases (CAs), the CA domain and a bridge domain linking the matrix arm and the CA domain (Maldonado et al., 2020; Soufari et al., 2020; Klusch et al., 2021). Genes encoding subunits of the CA domain are present in the genomes of many eukaryotes but not opisthokonts, suggesting that this

feature was present in LECA but has been lost in fungi and animals (Cainzos et al., 2021). Complex I oxidizes NADH at the tip of the matrix arm and transfers electrons via several iron-sulfur (Fe-S) clusters across this arm to reduce ubiquinone at the interface between the matrix and membrane arms (Lopez-Lopez et al., 2022). Concomitantly, protons are transferred from the matrix to the IMS by the membrane arm via an uncharacterized mechanism (Baradaran et al., 2013; Kampjut and Sazanov, 2020; Kolata and Efremov, 2021; Parey et al., 2021). In plants, complex I activity is essential as null mutants are unable to establish a seedling (Kühn et al., 2015) or are male-sterile (Gutierrez et al., 1997).

Complex I is one of the most studied OXPHOS complexes in plants (Braun et al., 2014); yet many aspects of its biology remain unclear. For example, its composition is not fully resolved as structural work indicates that at least one additional subunit would be present (Maldonado et al., 2020; Soufari et al., 2020; Klusch et al., 2021). In addition, little is known about the regulation of complex I activity *in planta*. In order to identify genes encoding mitochondrial proteins playing important roles for complex I function, we performed a gene function prediction approach using EnsembleNet (Hansen et al., 2018). One of the identified candidate genes encodes a mitochondrial protein belonging to the ferredoxin (FDX) family.

In eukaryotes, FDXs are conserved cysteinyl-ligated [2Fe-2S] proteins participating to a wide range of oxidation–reduction reactions. In plants, FDXs are present both in plastids and mitochondria (Takubo et al., 2003; Przybyla-Toscano et al., 2018). The chloroplastic isoforms are at a metabolic crossroad, controlling the electron flow towards CO<sub>2</sub> fixation, nitrogen and sulfur assimilation or lipid desaturation, for instance (Hanke and Mulo, 2013; Przybyla-Toscano et al., 2018). Concerning mitochondrial representatives, mFDX1 and mFDX2 have been associated with cofactor (i.e. biotin) and hormone (i.e. homocastasterone) biosynthetic pathways in *Arabidopsis* (*Arabidopsis thaliana*) (Picciocchi et al., 2003; Bellido et al., 2022); and more importantly, they should be involved in the *de novo* synthesis of Fe-S clusters by analogy with the model in other organisms (Przybyla-Toscano et al., 2021). They receive electrons from a mitochondrial NADPH-dependent FDX reductase (FDXR, also known as adrenodoxin reductase in animals). Functional analysis of *fdxr* mutants and double mutants *mfdx1 mfdx2* in *Arabidopsis* revealed that the function of this FDXR-FDX system is critical in mitochondria for female gametophyte development and for early embryogenesis through a maternal effect (Bellido et al., 2022). In *Arabidopsis*, a third gene encoding a putative FDX (At3g07480) has been identified in mitochondrial proteome studies (Heazlewood et al., 2004; Senkler et al., 2017; Fuchs et al., 2020; Niehaus et al., 2020). In green algae, the homologous protein was described as a complex I subunit (Cardol et al., 2004). Furthermore, the cryo-EM structure of complex I from *Arabidopsis* and the green alga *Polytomella* sp. identified this protein as a structural subunit present in the bridge domain linking the matrix arm and the CA domain (Klusch et al., 2021). However, one cysteine that normally

serves as Fe-S cluster ligand in classical FDXs is absent in this additional Arabidopsis FDX, and accordingly only a metal ion was observed in its structure despite it adopts the overall fold of FDX. Moreover, functional studies have not been performed for this protein *in planta*.

In this study, we performed an *in vitro* biochemical characterization of the recombinant Arabidopsis mFDX-like (AtmFDX-like), which demonstrated that mFDX-like does not coordinate an Fe-S cluster unless the missing cysteine is reincorporated. This suggests that mFDX-like is not involved in electron transfer reactions. Using CRISPR-Cas9 lines, we also showed that an Arabidopsis *mfdx-like* knock-out mutant does not exhibit any abnormal phenotype when grown under standard conditions. However, at the molecular level, we evidenced that mFDX-like is essential for the formation of complex I-containing respiratory supercomplexes in plant mitochondria.

## Results

### The atypical mFDX-like is present in several eukaryotic groups of the green lineage

To delineate the function of AtmFDX-like, we firstly analyzed and compared its protein sequence with the ones of mitochondrial FDX homologs from Arabidopsis, yeast (*Saccharomyces cerevisiae*), and human (*Homo sapiens*) (Supplemental Figure S1). Alignment of primary sequences revealed that Arabidopsis mFDX-like represents an atypical isoform sharing only approximately 20% sequence identity with Arabidopsis mFDX1/2, whereas Arabidopsis mFDX1 and 2 share 76% identity even when including their targeting sequences. Assuming that all these sequences diverged from a single ancestor gene, mFDX-like diverged substantially. In particular and as already mentioned, one of the 4 cysteines serving as ligands for the putative Fe-S cluster is absent, and 2 other cysteines are separated by 3 amino acids instead of 2 in regular FDXs. Moreover, most negatively charged residues known to be involved in the interaction with FDXR are not conserved, raising questions about its function(s) and partner(s). Standard PSI-BLAST searches using AtmFDX proteins as queries identified both classical and atypical mFDXs, despite the fact that mFDX-like proteins form a clade diverging from classical mFDXs, and obviously from plastidial FDXs (Figure 1). A careful inspection of mFDX-like distribution revealed that mFDX-like proteins are restricted to eukaryotes of the green lineage as demonstrated by their absence in cyanobacteria but presence in some algae, notably chlorophytes, as well as in bryophytes, lycophytes and angiosperms. The NUOP3 protein from *Chlamydomonas reinhardtii* that was previously shown to be also associated with complex I (Cardol, 2011) is in the same branch as AtmFDX-like (Figure 1) although they have diverged substantially, since both proteins have 20% identity (Supplemental Figure S2). Worth mentioning, most algal mFDX-like do not possess the 3 remaining cysteines known

to serve as Fe-S cluster ligands in regular FDXs, whereas they are still present in mFDX-like from terrestrial plants. This suggests their progressive loss during evolution and dispensability at least for a role as a complex I structural subunit. Intriguingly, the NDUFX protein present in the complex I structure from the free-living protozoa *Tetrahymena thermophila* belonging to the Ciliophora phylum (Zhou et al., 2022) is present in the same phylogenetic clade (Figure 1).

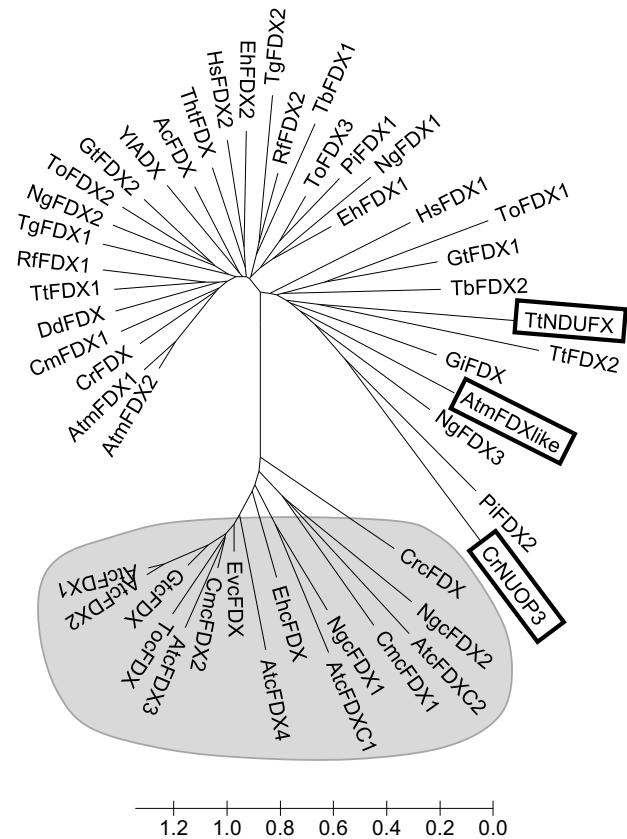


**Figure 1** The atypical mFDX-like proteins form a phylogenetic branch distinct from other eukaryotic FDXs. Protein sequences of FDXs were retrieved from a selection of eukaryotic organisms representing the different eukaryotic lineages (see Supplemental Table S1). Sequences were analyzed using MEGA (www.megasoftware.net), and a minimum evolution tree was built using default parameters. The optimal tree is shown. The tree is drawn to scale, with branch lengths in the same units as those of the evolutionary distances used to infer the phylogenetic tree. The evolutionary distances were computed using the Poisson correction method and are in the units of the number of amino acid substitutions per site. Plastid FDXs are shaded in grey. The 3 FDXs described as complex I subunits are shown with boxes. Ac, *Acanthamoeba castellanii*; At, *Arabidopsis thaliana*; Cm, *Cyanidioschyzon merolae*; Cr, *Chlamydomonas reinhardtii*; Dd, *Dictyostelium discoideum*; Eh, *Emiliania huxleyi*; Ev, *Euglena viridis*; Gi, *Giardia intestinalis*; Gt, *Guillardia theta*; Hs, *Homo sapiens*; Ng, *Nannochloropsis gaditana*; Pi, *Phytophthora infestans*; Rf, *Reticulomyxa flosa*; Tb, *Trypanosoma brucei*; Tg, *Toxoplasma gondii*; Th, *Thecamonas trahens*; To, *Thalassiosira oceanica*; Tt, *Tetrahymena thermophila*; Yl, *Yarrowia lipolytica*. The UniProt accessions of all the proteins analyzed are given in Supplemental Table S1.

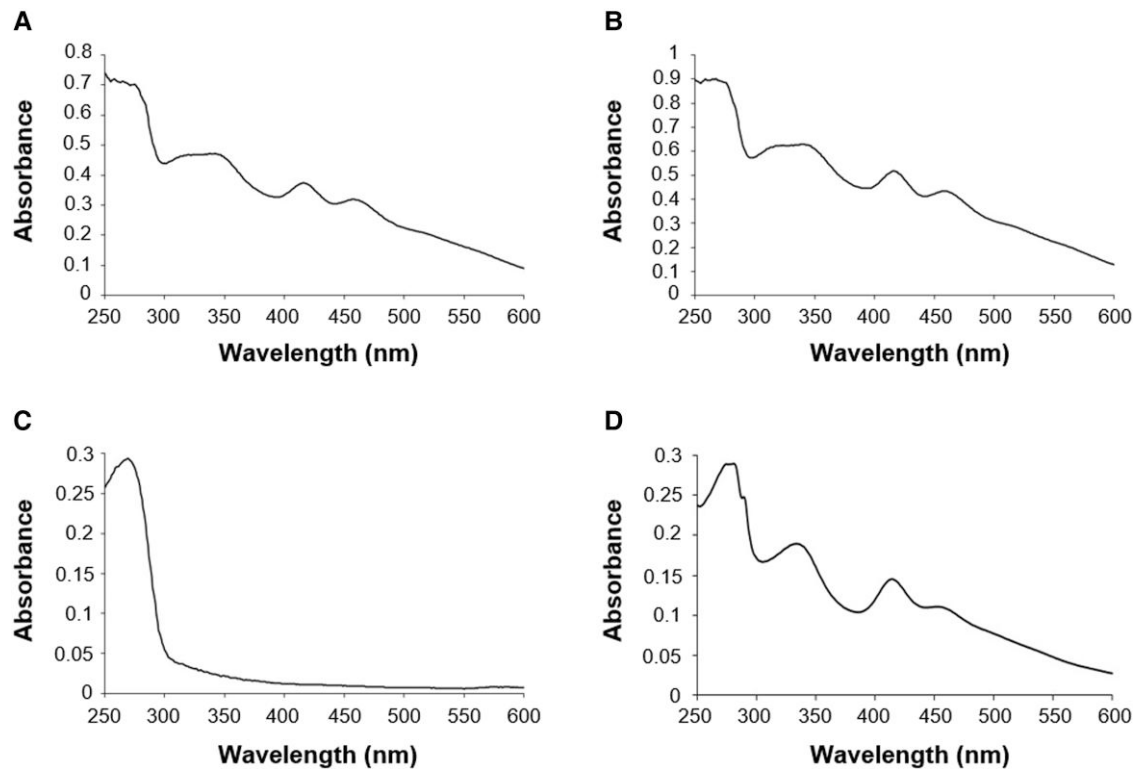


**Figure 2** mFDX-like does not coordinate an Fe-S cluster. UV-visible absorption spectra of as-purified *Arabidopsis thaliana* his-tagged mFDX1 (A), mFDX2 (B), mFDX-like (C), and mFDX-like L85C variant (D) recombinantly expressed in *E. coli*.

### The absence of a single cysteine residue prevents mFDX-like from binding the regular [2Fe-2S] cluster

From the 3D structure analysis of *Arabidopsis* mFDX-like, we noticed that a histidine residue, which may serve as an Fe-S cluster ligand in some proteins, is positioned in the region where the cysteine ligand normally is. In order to obtain clear evidence that this protein indeed lost the capacity to bind the [2Fe-2S] cluster normally present in classical mFDXs, we individually expressed the 3 *Arabidopsis* mFDXs in an *Escherichia coli* heterologous system, and purified the corresponding recombinant proteins (Supplemental Figure S3). After purification, only mFDX1 and mFDX2 exhibited a strong reddish-brown coloration. Accordingly, their UV-visible absorption spectra showed characteristic absorption bands at 342, 416, and 457 nm typical of the presence of a [2Fe-2S] cluster (Figure 2, A and B). In contrast, no similar absorption bands were visible for mFDX-like (Figure 2C), indicating that the histidine residue cannot substitute for the cysteine ligand. To understand whether more pronounced structural changes occurred or whether introducing a single cysteine residue is enough for restoring the [2Fe-2S] cluster binding capacity, we have also expressed a variant of mFDX-like in which the leucine at position 85 was replaced by a cysteine (L85C). In this case, the purified mutated variant showed an absorption spectrum comprising shoulders centered at 333, 414, and 452 nm, very similar to that observed for the [2Fe-2S] cluster-bound forms of mFDX1 and mFDX2 (Figure 2D). Altogether, these *in vitro* analyses indicate that the loss of a cysteine ligand

hampers [2Fe-2S] cluster binding by mFDX-like but that the protein still possesses the structural capacity to accommodate it when the cysteine is re-incorporated. In line with this, no [2Fe-2S] cluster was observed in *Arabidopsis* mFDX-like present in complex I structure but instead a single metal ion was coordinated by the residual cysteines and the histidine residue (Klusch et al., 2021).

### mFDX-like is a mitochondrial protein

The mFDX-like protein was reported in mitochondrial proteomes and in complex I structure (Klusch et al., 2021). To confirm that it is localized only in mitochondria *in vivo*, we generated stable *Arabidopsis* lines expressing a mFDX-like-GFP construct, and assessed its subcellular distribution by confocal laser microscopy. We observed that the mFDX-like-GFP signal colocalized nearly exclusively with the MitoTracker in root cells from 14-day-old seedlings, strengthening a “mitochondrion-only” targeting of the protein (Supplemental Figure S4). This corroborates earlier results obtained upon transient expression in cultured cells of *Arabidopsis* (Carrie et al., 2009).

### The absence of mFDX-like does not affect plant growth

To gain more insights into the physiological role of mFDX-like, we first searched for knock-out mutants from available *Arabidopsis* T-DNA insertion lines. Three lines were tested: *mfdxl-1*: SALK\_015333, *mfdxl-2*: WiscDsLoxHs204\_01A and

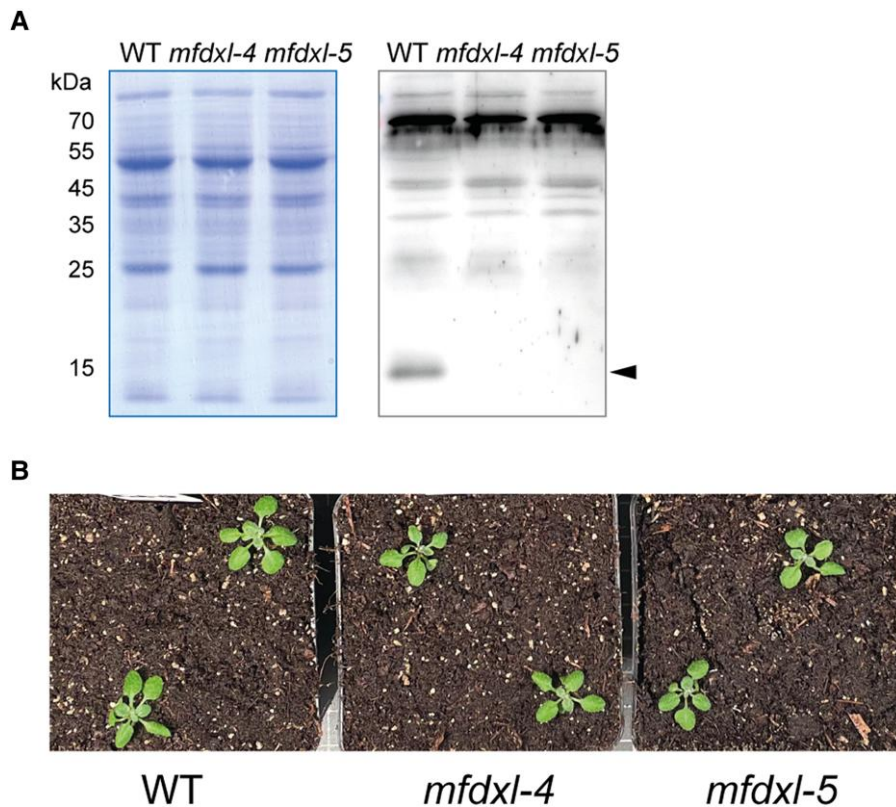


**Figure 3** The absence of mFDX-like does not affect plant growth. Two independent deletion lines were generated using the CRISPR-Cas9 genome editing technology. A, Mitochondria were isolated from the lines and mitochondrial proteins were analyzed by SDS-PAGE followed by immunoblot experiments using an anti-mFDX serum. Left panel: Coomassie staining of the membrane. Right panel: Signals obtained after incubation of the membrane using the anti-mFDX-like antibodies. The position of the mature form of mFDX-like is indicated by an arrowhead. The specific signals observed in the top part of the blot serve as loading control. B, Representation images of 20-day-old seedlings grown on soil under standard growth conditions.

*mfdxl-3*: SAIL\_37\_H11 (Supplemental Figure S5A). We could obtain homozygous lines for *mfdxl-1* and *mfdxl-2* but western blots performed with an antibody raised against mFDX-like indicated that these 2 lines did not have a loss or a decrease of mFDX-like when compared with wild-type (WT) plants (Supplemental Figure S5B and S5C). This was not so surprising as both T-DNA insertions are located in the 5' UTR. Furthermore, we were unable to isolate homozygous lines for *mfdxl-3* as this mutant showed an arrest in the development of some seeds in the siliques of the heterozygous plants (Supplemental Figure S5D). Therefore, we tested the viability of the pollen grain using Alexander's stain and observed that pollen-tetrads from the *mfdxl-3*<sup>-</sup> plant indeed contained some dead cells (Supplemental Figure S5D). To test whether the lack of mFDX-like was responsible for such drastic phenotype, we generated 2 independent deletion lines (*mfdxl-4* and *mfdxl-5*) using the CRISPR-Cas9 genome editing technology (Supplemental Figure S6). The mutants were backcrossed with WT plants to eliminate the Cas9 cassette and complemented by reintroducing the sequence coding for mFDX-like expressed under the constitutive 35S promoter in each line. The progeny from self-crossed plants was examined by western blot-based genotyping. Protein blot analysis on isolated mitochondria showed that the immune signal

corresponding to the mature form of mFDX-like (~ 15 kDa) was absent in both loss-of-function lines compared with WT plants (Figure 3A). Nevertheless, despite the absence of mFDX-like, none of these knock-out lines showed a growth phenotype when grown under standard conditions (Figure 3B). To assess the potential lethality due to a lack of mFDX-like observed in the *mfdxl-3* T-DNA mutant line, we transformed heterozygous *mfdxl-3* plants with the complementation construct but we failed to obtain any plant containing both T-DNAs. In addition, we failed to amplify both T-DNA::genome junctions, suggesting the presence of a genomic rearrangement, a phenomenon that occurs frequently in T-DNA insertion lines (Clark and Krysan, 2010; Pucker et al., 2021). Taken together, our results support the idea that the phenotype of *mfdxl-3* derives from a complex genomic alteration rather than from the lack of mFDX-like. Furthermore, this functional analysis demonstrated that mFDX-like is not essential for plant growth and development under standard growth conditions.

### mFDX-like is essential for supercomplex formation between complex I and complex III<sub>2</sub>

Since the mFDX-like protein has been described as a structural subunit of complex I (Klusck et al., 2021), we analyzed

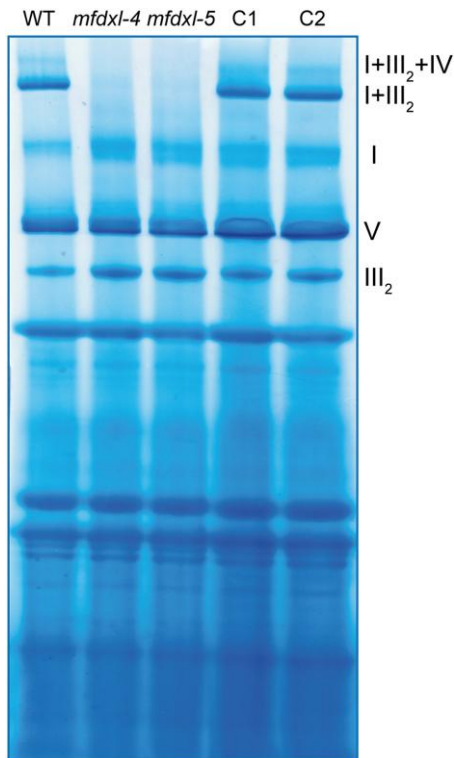


**Figure 4** mFdx-like is essential for supercomplex formation. Blue native PAGE analysis of mitochondrial complexes. Mitochondria were solubilized using digitonin and the complexes separated on a native gel. After migration, the gel was stained with Coomassie blue. OXPHOS complexes I, III<sub>2</sub>, and V and supercomplexes (I + III<sub>2</sub>, I + III<sub>2</sub> + IV) are indicated on the right. C1 and C2 are the complemented lines of mutants *mfdxl-4* and *mfdxl-5*, respectively.

complex I levels in *mfdxl-like* knock-out lines. To this end, mitochondria were isolated, complexes solubilized with digitonin, and separated under native electrophoresis conditions. The gel was then stained with Coomassie blue to visualize OXPHOS complexes. The bands corresponding to complex I, complex III dimer (III<sub>2</sub>), and complex V presented a similar intensity in the deletion lines in comparison with the WT and complemented lines (Figure 4). However, the bands corresponding to complex I-containing supercomplexes were not detectable in both knock-out lines (Figure 4). When mFdx-like was reintroduced, these supercomplexes were detectable again, demonstrating that mFdx-like is required for the formation of complex-I-containing supercomplexes in Arabidopsis.

### mFdx-like is important for the assembly of the membrane arm of complex I

To gain further insights into the role of mFdx-like in respiratory complex I formation, we performed additional native gels and transferred the multiprotein complexes on membranes (Figure 5A). Assembly intermediates and abundance of complex I were visualized by immunoblotting using antibodies recognizing certain subunits or assembly factors of the complex I.

As previously observed, no supercomplexes I + III<sub>2</sub> were detected in Arabidopsis cas9-edited lines when antibodies raised against the complex I subunit carbonic anhydrase 2 (CA2) were used. This confirmed the importance of mFdx-like for the formation of complex-I-containing supercomplexes. Interestingly, the absence of mFdx-like led to the appearance of additional bands of both larger and smaller size than the mature complex I (Figure 5B). To determine whether the additional bands detected with the anti-CA2 antibodies represented assembly intermediates or degradation products, we used anti-L-galactono-1,4-lactone dehydrogenase (GLDH) antibodies as GLDH is an assembly factor of complex I present in assembly intermediates but absent in mature complex I and its degradation products (Schertl et al., 2012; Schimmeyer et al., 2016; Ligas et al., 2019). The same band pattern was detected with the anti-CA2 or anti-GLDH antibodies in the deletion lines (Figure 5C). This indicated that these bands corresponded to assembly intermediates, and thus demonstrated that the assembly pathway of complex I is impaired in the absence of mFdx-like. Of note, the monomeric GLDH was not detected in the deletion lines while it was visible in both WT and complemented lines (Figure 5C; lower part of the native gel). The fact that the assembly intermediates were also slightly accumulated in the complementation lines compared with the WT line suggests that the complemented lines are not fully rescued.

Both anti-CA2 and anti-GLDH antibodies detect at least one band that is larger than complex I. Because of the presence of GLDH, this band likely contains the last and most stable assembly intermediate of complex I, complex I\* (Ligas et al., 2019). To test if such band could correspond to an association of complex I\* with complex III<sub>2</sub> (the observed size of this band corresponds to the expected size for such an association), we performed an immunoblot detection with antibodies raised against a subunit of mitochondrial complex III<sub>2</sub>, the Rieske iron-sulfur protein (RISP). In these conditions, no complex I-containing supercomplexes were detected but instead an increase in the abundance of a supercomplex slightly larger than complex V (Figure 5D). The largest GLDH-containing band is also not detected with the anti-RISP antibodies (Figure 5D), thus excluding that this band corresponds to a supercomplex I\*+III<sub>2</sub>. To gain further insights into the nature of the supercomplexes observed, we performed a cytochrome c oxidase activity staining of a replicate gel. Complex IV activity is detected in the central part of the gel and at the level of supercomplex III<sub>2</sub> + IV above complex V and of the supercomplex I + III<sub>2</sub> + IV at the top of the gel (Figure 5E). In addition, complex IV activity is detected between complex I and supercomplex I + III<sub>2</sub>. However, in contrast with the anti-CA2 and anti-GLDH signals detected in this area of the gel, this band is not increased in the *mfdxl* mutants, excluding that it represents a supercomplex containing complex I\* and complex IV (Figure 5E). This analysis demonstrates that mFdx-like is only essential for the formation of complex-I containing supercomplexes.

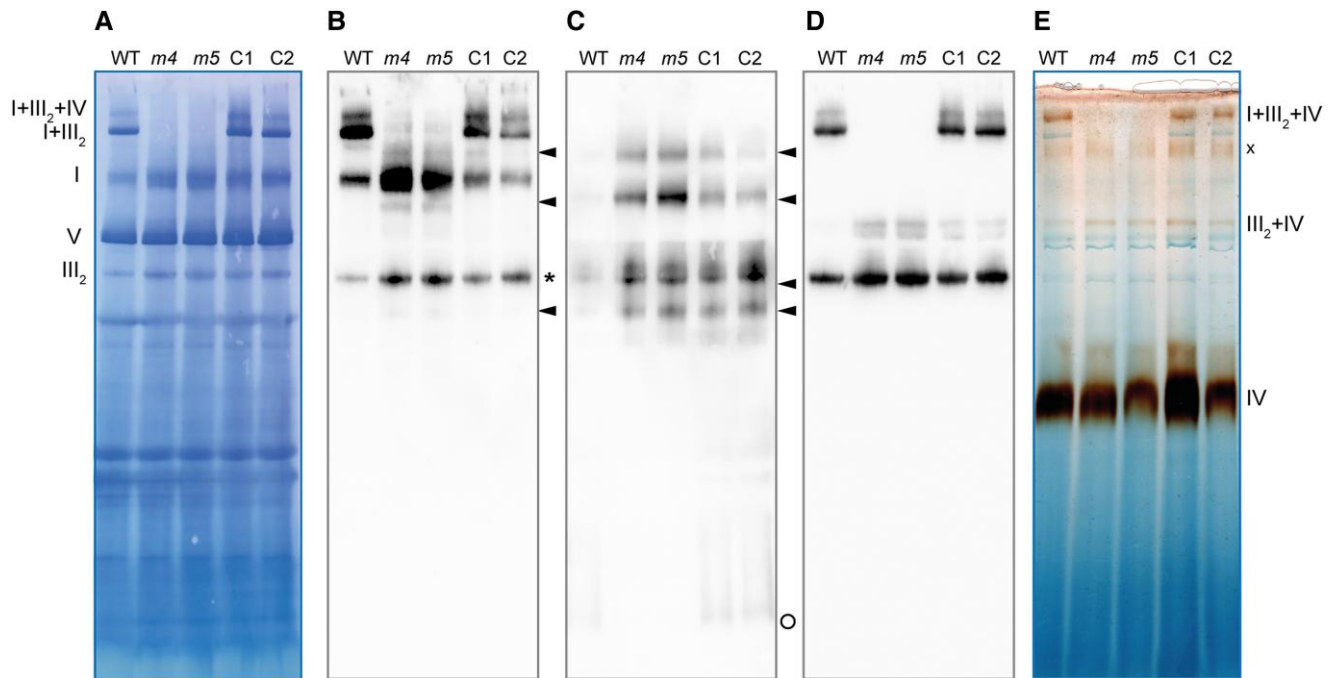


**Figure 5** mFDX-like is important for the assembly of complex I. Blue native PAGE analysis of mitochondrial complexes. Mitochondria were solubilized using digitonin and the complexes separated on a native gel. After migration, the complexes were transferred on a PVDF membrane which was used for immunoblot analyses. *m4*: *mfdxl-4*, *m5*: *mfdxl-5*. C1 and C2 are the complemented lines of the *mfdxl-4* and *mfdxl-5* mutants, respectively. A, Coomassie staining of the membrane after transfer, the position of the OXPHOS complexes and supercomplexes is indicated on the left (I: complex I, III<sub>2</sub>: complex III dimer, IV: complex IV, V: complex V). B, Signals obtained after incubation of the membrane with the anti-CA2 antibodies. Complex I related complexes accumulated in the deletion mutants are indicated with an arrowhead. \*: specific reaction of complex III<sub>2</sub> with the ECL reagent. C, Signals obtained after incubation of the membrane with the anti-GLDH antibodies. Complex I assembly intermediates are indicated with an arrowhead. Free GLDH running close to the bottom of the gel is indicated with a circle. D, Signals obtained after incubation of the membrane with the anti-RISP antibodies. The same membrane has been used to perform the 3 immunoblot analyses. E, Complex IV-activity staining of a replicate BN gel. x: unknown complex IV-containing supercomplex.

### CA2 is important for the assembly of the P<sub>D</sub> domain

Complex I\* lacks the P<sub>D</sub> module of the membrane arm. However, mFDX-like interacts with CAL2 of the CA domain and Nad2 of the P<sub>P</sub> module (Klusck et al., 2021); as such mFDX-like is not directly interacting with the P<sub>D</sub> module. Therefore, the accumulation of complex I\* in the deletion mutants cannot be explained by a direct role of mFDX-like in the assembly of the P<sub>D</sub> module. In plants, the association of the P<sub>D</sub> module with complex I\* requires the release of GLDH, that is associated with the P<sub>P</sub> module (Ligas et al., 2019). The structures of complex I\* (with GLDH) and complex I (without GLDH) in cauliflower (*Brassica oleracea*) show that the CA domain is shifted by 6 Å between both structures (Soufari et al., 2020). Therefore, a conformational rearrangement of the membrane arm of complex I\* is required to release GLDH and allow the binding of the P<sub>D</sub> module. Such rearrangement could be triggered by the formation of the bridge domain between the matrix arm and the CA domain of complex I\*. Based on this hypothesis, a mutant containing an altered CA domain that cannot shift should also be impaired in the assembly of the P<sub>D</sub> module. No assembly intermediates were detected in mutants lacking the CA subunits (Meyer et al., 2011). Nevertheless, assembly intermediates might be below the detection limit in such mutants as they accumulate very low

levels of complex I (Perales et al., 2005; Fromm et al., 2016). To overcome this issue, we crossed *ndufs4*, a mutant accumulating the membrane arm, the P<sub>P</sub> module and its assembly intermediates (Meyer et al., 2009; Kühn et al., 2015) with a *ca2* mutant in which the assembly of complex I is limited by the assembly of the CA domain. We performed reciprocal crosses to rule out a potential maternal effect, and obtained the *ndufs4 ca2* and *ca2 ndufs4* lines. We then analyzed the assembly of complex I using native gel electrophoresis followed by immunodetection of Nad6, a subunit of the P<sub>P</sub> module of complex I. In *ndufs4*, the full membrane arm can be assembled but in the double mutants, the membrane arm is not detectable, instead the P<sub>P</sub> module accumulates (Figure 6). This indicates that the assembly is stalled, and that the P<sub>D</sub> module cannot be efficiently associated with the P<sub>P</sub> module to form the membrane arm in the absence of CA2. Therefore, in addition to its role in the assembly of the P<sub>P</sub> module, CA2 is also needed for the correct assembly of the P<sub>D</sub> module.

### The role of mFDX-like in supercomplex formation is likely independent of NDUFA11

The structure of complex I-containing supercomplexes has been recently reported in plants (Klusck et al., 2023;

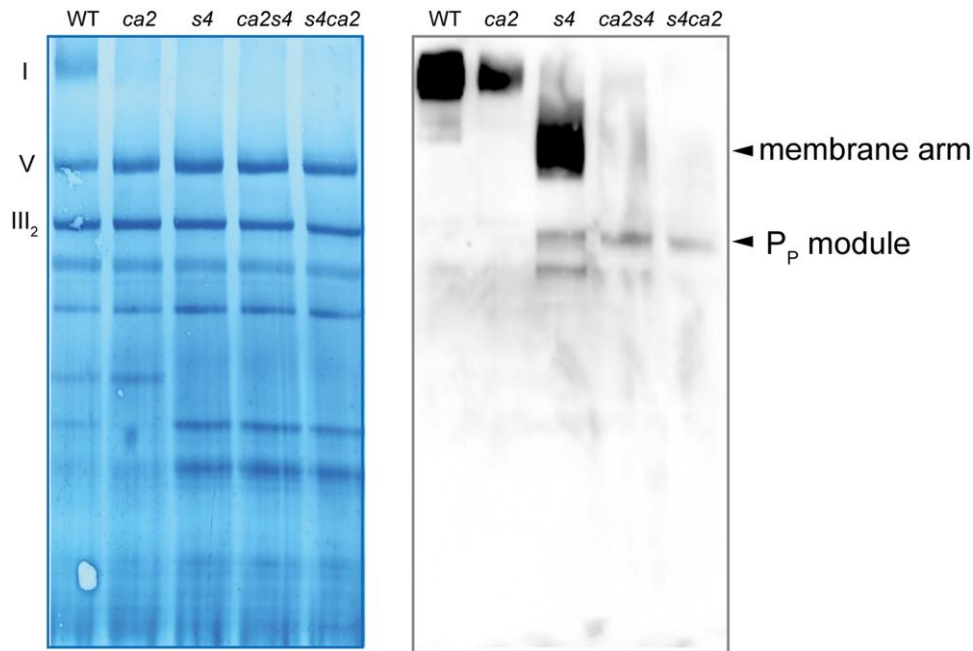


**Figure 6** CA2 is important for the assembly of the  $P_D$  module. Blue native PAGE analysis of mitochondrial complexes. Mitochondria were solubilized using dodecyl-maltoside and the complexes separated on a native gel. After migration, the complexes were transferred on a PVDF membrane which was used for immunoblot analyses. Left panel: Coomassie staining of the membrane after transfer, the position of the OXPHOS complexes is indicated on the left (I: complex I,  $III_2$ : complex III dimer, V: complex V). Right panel: Signals obtained after incubation of the membrane with the anti-Nad6 antibodies. Complex I assembly intermediates accumulating in the mutants are indicated on the right. *ca2*: mutant lacking the subunit CA2, *s4*: mutant lacking the subunit NDUFS4, *ca2s4* and *s4ca2*: double mutants lacking CA2 and NDUFS4.

Maldonado et al., 2023). Based on these structures and the ones of supercomplexes I +  $III_2$  isolated from mammalian (Gu et al., 2016; Letts et al., 2019) or from Tetrahymena (Zhou et al., 2022), 2 main contact sites between complex I and complex  $III_2$  have been highlighted. The first one is formed by the NDUA11 subunit of complex I and the UQCRB (QCR7) subunit of complex  $III_2$  whereas the second one occurs between the NDUB4 and NDUB9 subunits of complex I and the UQCRC1 (MPPbeta) subunit of complex  $III_2$  (Letts et al., 2019). NDUA11 is not present in the structure of Arabidopsis complex I (Soufari et al., 2020) but if its binding site is conserved between opisthokonts and plants, NDUA11 should be located just underneath mFDX-like. Hence, a possible role of mFDX-like could be to stabilize NDUA11. If this is true, NDUA11 would be unable to mediate the interaction with complex  $III_2$  in the absence of mFDX-like, leading to the absence of the supercomplex I +  $III_2$ . To test this hypothesis, we isolated a homozygous T-DNA insertion line in the *NDUA11* gene. In these plants, NDUA11 gene product was not detected from isolated mitochondria by immunoblot assay using specific antibodies (Michaud et al., 2016) (Figure 7A). Yet, the Arabidopsis *ndua11* knock-out mutant showed normal growth and development when compared with WT plants (Figure 7B). Despite the absence of a macroscopic phenotype, we checked whether a *ndua11* mutant could be affected in OXPHOS complexes using native gel electrophoresis coupled with immunoblot analyses.

Similar to what was observed in a *mfdx-like* mutant, complex I-containing supercomplexes were undetectable in the absence of NDUA11 (Figure 7C), confirming that NDUA11 is essential for the interaction between complex I and complex  $III_2$  within the supercomplex. We next tested if the absence of mFDX-like could disturb the recruitment of NDUA11 in the respiratory complex I. For this purpose, immunoblot analysis with anti-NDUA11 antibodies was assayed on separated OXPHOS complexes from WT and *mfdx-like* plants. In all genetic backgrounds, NDUA11 was associated with complex I (Figure 7D). Therefore, the absence of supercomplexes I +  $III_2$  in *mfdx-like* knock-out lines does not result from the absence of NDUA11.

## Discussion

### Evolution of the function of mFDX-like

According to our phylogenetic analysis, Arabidopsis FDXs from eukaryotic organisms are grouped into 3 clades: the plastidial FDXs, the classical mitochondrial FDXs, and a clade containing both classical and divergent mitochondrial FDXs (based on the presence or the absence of one or more of the cysteines required for the coordination of the Fe-S cluster) that includes mFDX-like and the 2 other FDXs previously shown to be associated with complex I. Interestingly, additional putative orthologs are present in this branch and



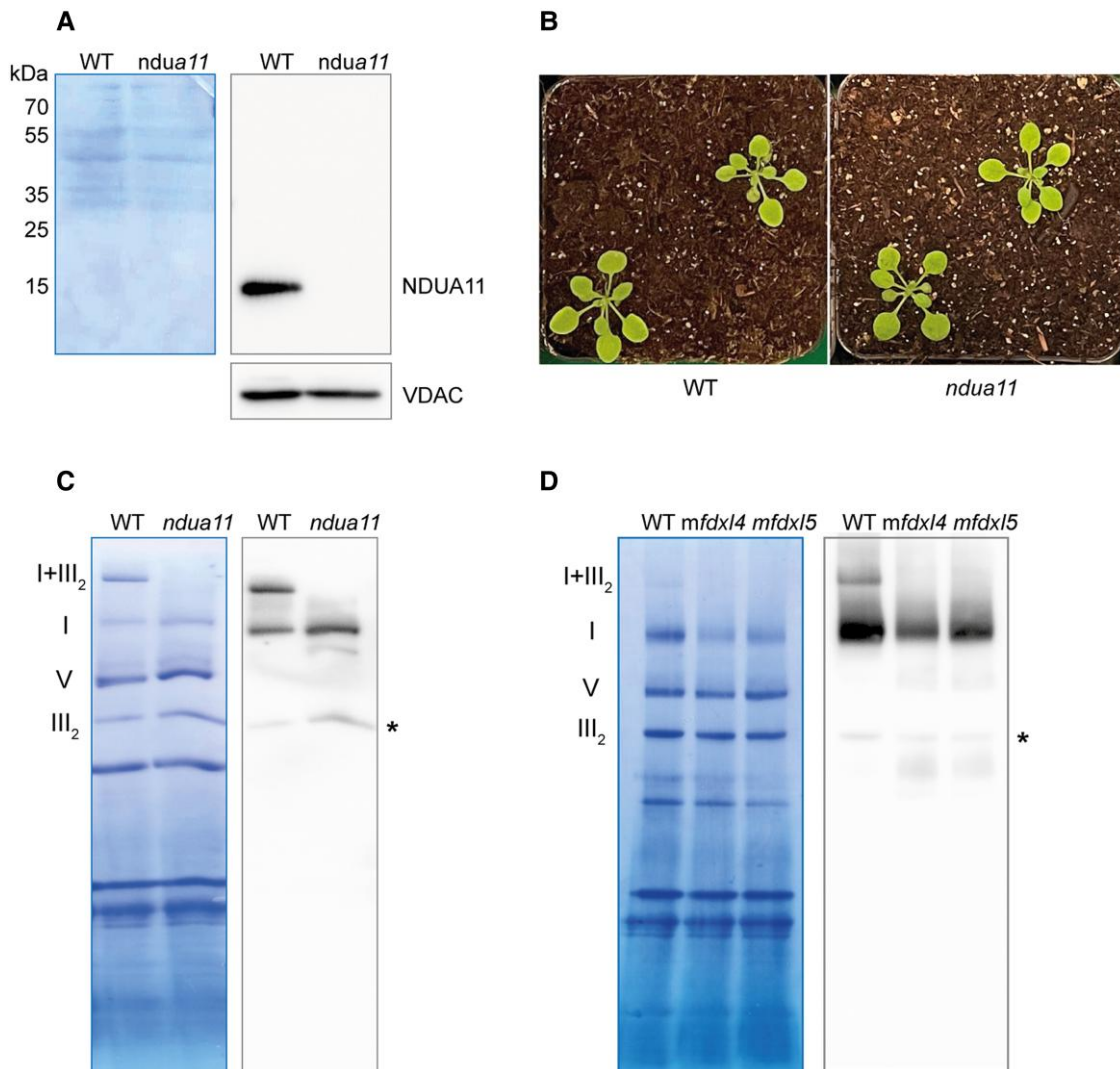


**Figure 7** NDUA11 is essential for supercomplex formation but its association with complex I is not affected in *mfdx1* mutants. **A**. Mitochondria were isolated from the *ndua11* and WT plants and mitochondrial proteins were separated by SDS-PAGE and analyzed by immunoblot analyses. Left panel: Coomassie staining of the membrane. Right panels: Signals obtained after incubation of the membrane with first the anti-NDUA11 antibodies and second the anti-VDAC antibodies. The detection of VDAC is used as a loading control. **B**. Image of 20-day-old seedlings grown on soil under standard growth conditions. **C**. Blue native PAGE analysis of mitochondrial complexes. Mitochondria were solubilized using digitonin and the complexes separated on a native gel. After migration, the complexes were transferred on a PVDF membrane which was used for immunoblot analyses. Left panel: Coomassie staining of the membrane after the transfer, the position of the OXPHOS complexes is indicated on the left (I + III<sub>2</sub>: supercomplex I + III<sub>2</sub>, I: complex I, III<sub>2</sub>: complex III dimer, V: complex V). Right panel: signals obtained after incubation of the membrane with the anti-CA2 antibodies. \*: aspecific reaction of complex III<sub>2</sub> with the ECL reagent. **D**. Blue native PAGE analysis of mitochondrial complexes. Mitochondria were solubilized using digitonin and the complexes separated on a native gel. After migration, the complexes were transferred on a PVDF membrane which was used for immunoblot analyses. Left panel: Coomassie staining of the membrane after the transfer, the position of the OXPHOS complexes is indicated on the left (I + III<sub>2</sub>: supercomplex I + III<sub>2</sub>, I: complex I, III<sub>2</sub>: complex III dimer, V: complex V). Right panel: signals obtained after incubation of the membrane with the anti-NDUA11 antibodies. \*: aspecific reaction of complex III<sub>2</sub> with the ECL reagent.

represent potential candidates for complex I-associated FDXs. However, this would have to be experimentally validated. Also, this clade contains proteins from organisms belonging to distinct eukaryotic groups (Supplemental Table S1), suggesting that the association of an FDX with complex I is an ancestral feature of this complex.

The *in vitro* characterization of *Arabidopsis* mFDX-like demonstrated that it does not bind an Fe-S cluster according to

the lack of a cysteine ligand. Hence, mFDX-like does not behave as a classical FDX, and its involvement in electron transfer reactions is unlikely. The absence of cysteine ligands in most algal mFDX-like suggests that these residues do not have an important structural or functional role. Still, because most cysteines have been conserved during evolution in mFDX-like from terrestrial plants, it would be interesting to test whether they might be important for the role of

mFDX-like in these organisms, for instance by making functional complementation assays. Altogether these phylogenetic and biochemical data suggest that the function of mFDX-like has likely evolved from a conventional enzymatic electron transfer function towards a strictly structural one.

It is worth mentioning that mFDX-like has never been identified as a complex I subunit in proteomic studies in *Arabidopsis*. This likely results from the consequence of the use of native gel electrophoresis as the bridge domain was only observed so far in sample preparations that do not include gel electrophoresis. Based on the analysis of the number of protein copies in a single mitochondrion, mFDX-like is an abundant protein, being present at levels globally similar to other complex I subunits and much more abundant than the 2 regular mFDX1/2 (Fuchs et al., 2020). Also, the transcript expression pattern of mFDX-like in plant organs or tissues of *Arabidopsis* is similar to the one of Fe-S cluster binding complex I subunits (Przybyla-Toscano et al., 2021). However, it remains to be determined whether mFDX-like is exclusively associated with respiratory complex I or if it can also play independent, non-essential roles as a soluble protein in the mitochondrial matrix.

### Assembly of complex I

In the *mfdxl* knock-out lines, no alteration of complex I levels has been observed but several assembly intermediates accumulate (Figure 5). We used 2 different antibodies to detect these intermediates, the anti-CA2 and anti-GLDH antibodies. CA2 is a subunit of the CA domain that is assembled early and is attached on the P<sub>p</sub> module of the membrane arm of complex I. GLDH is an assembly factor that is associated with 3 assembly intermediates including the P<sub>p</sub> module and complex I\* that is formed by the attachment of the almost fully assembled matrix arm on the P<sub>p</sub> module (Ligas et al., 2019). The accumulation of complex I\* in the *mfdxl* deletion lines indicates that the final step of the assembly is impaired. Thus, mFDX-like should be associated with complex I\* to proceed to the next step of the assembly. This step is the binding of the distal part of the membrane arm, the P<sub>D</sub> module. For this to occur, GLDH must be removed, the P<sub>D</sub> module attached to complex I\* and the NDUP1 subunit be bound across the P<sub>D</sub> and P<sub>p</sub> modules at the position where GLDH was bound (Meyer et al., 2022). We observed an absence of free GLDH in the *mfdxl* deletion lines, indicating that the bridge domain is important for the release of GLDH from complex I assembly intermediates. However, as complex I can be fully assembled in the *mfdxl* deletion lines, the release of GLDH can occur in the absence of mFDX-like but this step appears less efficient in the deletion lines than in WT plants. Our data demonstrate that mFDX-like is important for the transition from complex I\* to complex I.

The analysis of the two reciprocal double mutants lacking NDUF54 and CA2 also points towards a role of CA2 in the assembly of the P<sub>D</sub> module and suggests that mFDX-like and the CA domain are important for the efficient assembly of the P<sub>D</sub> module. The structural characterization of complex

I and complex I\* in cauliflower supports a common function of mFDX-like and the CA domain in the transition from complex I\* to complex I. The position of the CA domain was found to be shifted by 6 Å towards the missing P<sub>D</sub> module between complex I and complex I\* (Soufari et al., 2020). A possible mechanism integrating all these results would be that upon building of the bridge domain (binding of mFDX-like), the CA domain is pushed away by 6 Å, allowing the release of GLDH from complex I\* and the binding of the P<sub>D</sub> domain.

In *ca2*, the CA domain is present and looks similar than in WT (Sunderhaus et al., 2006), indicating that CA2 is replaced by another CA subunit. This might affect the attachment of the CA domain on the membrane as the N-terminal  $\alpha$ -helix of CA2 is involved in the interaction between the CA domain and the P<sub>p</sub> module (Maldonado et al., 2020; Soufari et al., 2020; Klusch et al., 2021). Low levels of complex I and supercomplex I + III<sub>2</sub> can be assembled in *ca2* (Perales et al., 2005; Fromm et al., 2016), indicating that the unusual CA domain in *ca2* remains limiting for the assembly but the assembly process is not disturbed. However, in the *ndufs4 ca2* double mutants, the binding of the P<sub>D</sub> module on the P<sub>p</sub> module is impaired (Figure 6). The main difference between *ca2* and the *ndufs4 ca2* mutants is the presence or absence of the matrix arm. This suggests that, when the CA domain does not contain CA2, the matrix arm should be attached to the P<sub>p</sub> domain to allow the binding of the P<sub>D</sub> domain. Whether or not this is linked to the formation of the bridge domain between the matrix arm and the CA domain remains to be explored.

In summary, both the bridge domain including mFDX-like and the CA domain are important for complex I assembly as the bridge domain likely influences the positioning of the CA domain on the P<sub>p</sub> module, the release of GLDH and the binding of the P<sub>D</sub> domain. However, mFDX-like is not directly responsible for the release of GLDH as GLDH removal and complex I assembly can occur in the deletion lines, albeit inefficiently. However, the complex I accumulating in these lines should have a different conformation than the one in the WT line, with the P<sub>D</sub> module being misoriented. Unfortunately, this cannot be currently tested as structural work in *Arabidopsis* has, to date, only been successful using cell cultures as starting material.

### Formation of supercomplexes

Based on the observation that complex I-containing supercomplexes are undetectable in the *mfdxl* deletion lines, we concluded that the complex I that accumulates is unable to associate with complex III<sub>2</sub>. This suggests either that mFDX-like is involved in the interaction with complex III<sub>2</sub> or that it is important for the formation of one of the contact points between both complexes. Tomography imaging revealed that the angle between complex I and complex III<sub>2</sub> is larger in plants than in opisthokonts (Davies et al., 2018). As the bridge domain of complex I faces complex III<sub>2</sub>, this could explain why more space is required between both

complexes. Recently, the structure of the supercomplex I + III<sub>2</sub> from *Tetrahymena* has been solved (Zhou et al., 2022). The bridge domain of complex I also contains a FDX, but also additional proteins that interact with complex III<sub>2</sub> subunits. Hence, it is possible that a similar organization exists in plants as well and that additional uncharacterized proteins present in the bridge domain and in the supercomplex I + III<sub>2</sub> remain to be identified in plants.

Two main contact points have been described at the level of the membrane arm. First, the complex I NDUA11 subunit interacts with UQCRB (QCR7) from complex III<sub>2</sub>. In the *Tetrahymena* supercomplex I + III<sub>2</sub> structure, these 2 subunits coordinate a zinc atom together (Zhou et al., 2022). The second contact point is between NDUB4 and NDUB9 subunits of the P<sub>D</sub> module and UQCRC1 (MPP-β) from complex III<sub>2</sub> (Letts et al., 2019). We have shown that NDUA11 is essential for supercomplex formation but also that NDUA11 is still present in the complex I that accumulates in the *mfdxl* deletion lines. In addition, our data suggest that the assembly of the P<sub>D</sub> module is dependent on structural rearrangements triggered by mFDX-like. Altogether, these results point towards a structural role for mFDX-like to correctly position either NDUA11 or the P<sub>D</sub> module. In the absence of mFDX-like, the P<sub>D</sub> domain can still associate with complex I\* but its position would be shifted, impairing the association with complex III<sub>2</sub>. As NDUA11 interacts with an α-helix of the subunit Nad5 in the P<sub>D</sub> module, an inadequate position of the P<sub>D</sub> module might influence the positioning of NDUA11 and also disturb the interaction with complex III<sub>2</sub>. Overall, we propose that mFDX-like and the bridge domain are essential for the correct organization of the membrane arm of complex I. To test further this hypothesis, the determination of the structure of complex I in the *mfdxl* deletion lines would be required.

## Conclusion

We previously identified mFDX-like through a bioinformatic screen aimed at identifying genes encoding mitochondrial proteins involved in complex I proteostasis (Hansen et al., 2018). More recently, structural analyses described mFDX-like proteins from *Arabidopsis* and the green alga *Polytomella* as structural subunits of respiratory complex I (Klusch et al., 2021), reinforcing our predictions and demonstrating the robustness of this initial bioinformatic approach. In this work, we provide insights into the biochemical properties and importance of mitochondrial FDX-like in the assembly pathway of the plant respiratory complex I as well as in the establishment of complex I-containing supercomplexes. This suggests a key role for mFDX-like in the conformation of the membrane domain. The recently obtained structures of plant supercomplex I + III<sub>2</sub> confirm the importance of mFDX-like and the bridge domain for the conformation of the membrane arm of complex I (Klusch et al., 2022; Maldonado et al., 2022).

Interestingly, the fact that the absence of mFDX-like had no influence on plant growth under standard growth

conditions supports the idea that complex I-containing supercomplexes are dispensable for plant growth. Yet, future studies should aim at challenging the physiological function of respiratory supercomplexes in plants under stress, and several of the mutant lines we have created would thus represent valuable tools for these investigations.

## Materials and methods

### Sequence alignments and phylogenetic analysis

*Arabidopsis* (*Arabidopsis thaliana*) mFDX protein sequences were retrieved from the *Arabidopsis* information resource (TAIR). Yeast and human mFDX amino acid sequences were collected from the Uniprot database (release 2022\_03), whereas the complete protein sequences corresponding to *Arabidopsis* mFDX-like putative orthologs were obtained using AtmFDX-like as a reference sequence and BLASTP tools at the Phytozome (v13) database. To retrieve the FDX sequences in selected eukaryotes (Supplemental Table S1), PSI-Blast searches were performed using mFDX1, mFDX2 or mFDX-like as baits. Phylogenetic and molecular evolutionary analyses were conducted using MEGA version 11 (Tamura et al., 2021). Multiple sequence alignments were performed with the multiple sequence comparison by log- expectation (MUSCLE) program using default parameters. The phylogenetic tree was constructed with the minimum-evolution option using default parameters. Final graphic views of the aligned sequences were generated with the BioEdit software (version 7.2.5).

### Expression of recombinant proteins and in vitro biochemical assays

The sequences encoding the presumed mature forms of mFDX-like (AA 37–159), mFDX1 (AA 70–197), and mFDX2 (AA 71–197) proteins were amplified from cDNA prepared from *A. thaliana* Col-0 leaf total RNA. Primers used are listed in Supplemental Table S2. The PCR products were cloned into pET15b expression vector (Novagen) between NdeI and BamHI restriction sites, resulting in the introduction of a hexa-His tag at the N-terminus of the expressed proteins. Site-directed mutagenesis was performed to substitute the leucine at position 85 by a cysteine using 2 mutagenic primers and standard circular PCR on the pET15b-mFDX-like vector (Supplemental Table S2). Expression of proteins in the *E. coli* BL21(DE3) pSBET strain transformed with recombinant pET15b plasmids was induced at exponential phase with 100 μM of isopropyl β-D-1-thiogalactopyranoside during 4 h at 37°C in 2.4 l cultures. Bacteria were then collected by centrifugation at 6,000 g during 20 min and resuspended in 30 mM Tris-HCl pH 8.0, 200 mM NaCl, 10 mM imidazole lysis buffer and eventually conserved at –20°C. Cell lysis was completed by 3 cycles of 1 min sonication on ice and the soluble fraction was separated from insoluble fractions and cellular debris by centrifugation at 40000 g during 40 min. The soluble fractions were loaded on a Ni-NTA

(Ni<sup>2+</sup>-nitrilotriacetate)–agarose resin equilibrated with a 30 mM Tris–HCl pH 8.0, 200 mM NaCl, 10 mM imidazole buffer. After a washing step, elution of captured His-tagged proteins from the column is accomplished by using the same buffer containing 250 mM imidazole. The fractions containing the proteins of interest were pooled, concentrated and imidazole was removed by repeated cycles of ultrafiltration using a YM10 membrane in an Amicon cell under nitrogen pressure. Purity and integrity of purified recombinant proteins were analyzed by 15% (w/v) SDS/PAGE (Supplemental Figure S3). Protein concentrations were determined by measuring the absorbance at 280 nm and using theoretical molar absorption coefficients of 2980 M<sup>-1</sup> cm<sup>-1</sup> for AtmFDX1 and AtmFDX2 and of 15,470 M<sup>-1</sup> cm<sup>-1</sup> for AtmFDX-like and AtmFDX-like L85C.

### Confocal laser microscopy imaging

Fragments comprising 1,000-bp region located upstream of the ATG translation start codon of *mFDX-like* gene to last codon before stop codon were amplified from WT genomic DNA using primers listed in Supplemental Table S2 and cloned into pGWB4 vector (Invitrogen). After *Agrobacterium*-mediated plant transformation, progenies were selected on ½ MS plates containing 0.7% (w/v) phytoagar, 50 µg/ml hygromycin antibiotic, and then cultivated in soil. Two-week-old roots grown on a ½ MS (0.8% (w/v) agarose) media were vacuum infiltrated with 100 nM of Mitotracker Orange CMTMRos (ThermoFischer, M7510), diluted in ½ MS, for 5 min and incubated 15 min in darkness. Fluorescence of the *mFDX-like*-GFP fusion protein and Mitotracker was observed with a confocal laser microscope (Zeiss, LSM780) using the Zeiss Zen software. GFP was detected using an Argon-laser (emission 488 nm/collection window 495–535 nm) with a gain at 750, and Mitotracker using a solid state laser (emission 561 nm/collection window 575–630 nm) with a gain at 420. Pictures were analyzed using the ImageJ software (<https://imagej.nih.gov/ij/>) where only contrast and brightness were adjusted.

### Obtention of plant lines

The T-DNA lines SALK\_015333, SAIL\_434\_E06, and WiscDsLoxHs204\_01A were obtained from the Nottingham Arabidopsis Stock Center and homozygous seedlings were obtained after selfing and confirmed by genotyping. CRISPR-Cas9 was used to create deletions in the gene encoding *mFDX-like* (Supplemental Figure S6A). First, to generate the PCR template pJF1033, the two sgRNA encoding cassettes were amplified from plasmid pHEE2E-TRI (Wang et al., 2015) with primers oJF212 and oJF215, the PCR product digested with HindIII and SpeI and ligated into equally cut pGGZ001 (Lampropoulos et al., 2013). The pair of guide RNAs was cloned in the pJF1031 vector (Ruf et al., 2019) that allows the expression of Cas9 under an egg-cell-specific promoter. First PCR primers containing the guide RNAs (oJF398 and oJF399) were used to amplify a fragment of the pJF1033 plasmid and the PCR product was inserted

into the Bsal sites of pJF1031. The resulting binary plasmid, pJF1120 (protospacer sequences AAACCGAAAAGTGAG TGA & TGCGAGGTTTCAGATCGCAG), is identical to pHEE2E-TRI except for the protospacer parts of the guide RNAs. pJF1120 was used to transform *Agrobacterium tumefaciens* GV3101 and the resulting bacteria were used to transform WT Col-0 plants by floral dip. Seeds of the T0 plants were screened on hygromycin. Resistant T1 plants were screened by PCR to detect deletion in the *mFDX-like* gene using primers mFDX1\_ScrF and mFDX1\_ScrR. Heterozygous plants were selfed and their progeny screened to obtain homozygous plants in which the WT allele is not detectable anymore by PCR (Supplemental Figure S6B). Sequencing of the PCR products obtained from the mutant plants identified two independent deletions (Supplemental Figure S6C). Both lines were backcrossed with WT plants to remove the Cas9 cassette and homozygous deletion mutants were screened by PCR. The elimination of the Cas9 cassette was confirmed by PCR using primers to detect Cas9 (Cas9\_F and Cas9\_R) and by testing the sensitivity to hygromycin of the back crossed homozygous lines. The two lines were named *mfdxl-4* and *mfdxl-5*. For the complementation, the genomic region corresponding to the coding sequence of *mFDX-like* was amplified by PCR using primers mFDX1\_ComF and mFDX1\_ComR and cloned into the pGWB2 vector. The resulting vector was transformed into *Agrobacterium tumefaciens* GV3101 and this strain was used to transform the two deletion lines by floral dip. Transformants were screened on hygromycin. A hygromycin sensitivity test was performed on T3 plants to identify complemented lines homozygous for the complementation construct. The sequences of all the primers used are given in Supplemental Table S2.

### Plant cultivation

Seeds were surface sterilized with ethanol 70% (v/v) containing 0.05% (v/v) Tween 20 and plated on MS media containing 1% (w/v) sucrose. Plates were incubated under long day conditions (16 h light 120 µE, 22°C and 8 h darkness, 20°C, the humidity was not controlled and oscillated between 40% and 65%). 10-day-old seedlings were transferred on soil and grown under the same long day conditions.

### Pollen viability assay

Inflorescences were collected from 6-week-old plants and fixed in a 6 ethanol:3 chloroform: 1 glacial acetic acid) during 3 h. After drying, flowers or buds were dissected, placed on microscope slide and anthers were stained with a modified Alexander's stain composed of 9.5% (v/v) ethanol, 0.01% (w/v) malachite green, 25% (v/v) glycerol, 0.05% (w/v) acid fuchsin, 0.005% (w/v) Orange G, and 4% (v/v) glacial acetic acid (Peterson et al., 2010). Preparations were quickly heated and observed under a light microscope (Zeiss Axio Observer.A1m equipped with an HBO 100 camera).

### Mitochondrion isolation

Mitochondria were isolated from 4-week-old plants according to (Meyer et al., 2009). Briefly, the aerial parts of the plant were ground in extraction buffer (0.3 M sucrose, 15 mM potassium pyrophosphate, 2 mM EDTA, 10 mM  $\text{KH}_2\text{PO}_4$ , 1% (w/v) polyvinylpyrrolidone-40, 1% (w/v) bovine serum albumin, 20 mM sodium ascorbate, pH 7.5) in a cold mortar. After filtration, 2 rounds of differential centrifugations (2000 g/20000 g) were performed to obtain a mitochondria-enriched pellet. After resuspension in wash buffer (0.3 M sucrose, 1 mM EGTA, 10 mM MOPS/KOH pH 7.2), the fraction was loaded on a discontinuous Percoll gradient comprised of 3 layers (18%–25%–50%) which was centrifuged at 40000 g for 45 min. The mitochondria were collected at the interface between the 25% and 50% layers and the Percoll was eliminated by performing several washes in wash buffer. Protein concentration was estimated using the Bradford assay (Rotiquant, Roth).

### Gel electrophoresis, blotting and activity staining

For the SDS-PAGE analysis, 10  $\mu\text{g}$  of mitochondrial proteins were loading on a 12% (w/v) acrylamide gel. After migration, the proteins were transferred on a PVDF membrane (Immobilon-P, Millipore) using a wet blotting system. For the BN-PAGE, 100  $\mu\text{g}$  of mitochondrial proteins were solubilized with either 5% (w/v) digitonin or 1% (w/v)  $\beta$ -D-dodecyl-maltoside and solubilized protein complexes were separated on a BN gel according to (Eubel et al., 2005). For some experiments, protein solubilization was performed directly after the isolation of mitochondria whereas for other experiments, mitochondria were stored frozen between isolation and solubilization. This storage step damages the supercomplexes and lower amounts of supercomplexes are detectable (Figures 6 and 7). After migration, the complexes were transferred on PVDF membrane (Immobilon-P, Millipore) using a wet blotting system. After transfer, the membranes were stained for 5 min in staining buffer (30% (v/v) methanol, 7% (v/v) acetic acid, 0.005% (w/v) Coomassie Blue R250). The background was reduced by washing the membranes in 30% (v/v) methanol, 7% (v/v) acetic acid. The stained membrane was scanned and the staining was fully removed using 100% (v/v) methanol. The in-gel complex IV activity staining was performed according to (Sabar et al., 2005). In brief, the 1D BN-gel was rinsed with water 3 times and incubated in staining solution without cytochrome *c* (10 mM phosphate buffer pH 7.4, 1 mg/ml 3,3'-diamino benzidine tetrahydrochloride dehydrate, 75 mg/ml saccharose, 19 U/ml catalase) for 30 min. The solution was replaced with fresh staining solution, containing 0.4 mg/ml cytochrome *c* and incubated until brown bands were clearly visible (3–23 h at RT).

### Antibody production and western blot

Polyclonal antibodies were produced in rabbits against the purified mFDX-like (Agrobio, France) or the peptide

RALRKKYARKDEDY specific to CA2 (Biogenes, Germany). The final bleeds were used for western blots. For western blot experiments, membranes were first blocked using a 5% (w/v) milk solution and incubated with the primary antibodies for 16 h at 4°C. Following 3 washes with TBS-T (20 mM Tris-HCl pH 7.4, 150 mM NaCl, 0.1% (v/v) Tween 20), the membranes were incubated with the secondary antibodies conjugated with HRP for 1 h at 4°C and again washed 3 times with TBS-T. Final detection was performed using the ECL prime detection reagent (Cytiva Amersham) and a CCD camera (Fusion FX, Vilber). The primary antibodies were used at the following dilutions: anti-mFDX-like 1/5000, anti-CA2 1/10000, anti-GLDH (Agrisera AS06182) 1/5000, anti-GDC-H (Agrisera AS05074) 1/1000, anti-RISP (Carrie et al., 2010) 1/10000, anti-Nad6 (Koprivova et al., 2010) 1/5000 and anti-NDUA11 (Michaud et al., 2016) 1/20000 and anti-VDAC (Blake et al., 2007) 1/10000.

### Accession numbers

Accession numbers are as follows: AT3G07480: mFDX-like, AT4G05450: mFDX1, AT4G21090: mFDX2, AT1G47260: CA2, AT5G67590: NDUS4, AT2G42210: NDUA11.

### Supplemental data

The following materials are available in the online version of this article.

**Supplemental Figure S1.** Amino acid sequence alignment of AtmFDX-like with mitochondrial ferredoxin homologs.

**Supplemental Figure S2.** Amino acid sequence alignment of selected plant and algal mFDX-like proteins.

**Supplemental Figure S3.** Purification steps and purity degree of recombinant proteins.

**Supplemental Figure S4.** Subcellular localization of AtmFDX-like in Arabidopsis.

**Supplemental Figure S5.** Genetic analysis and characterization of *mfdx-like* T-DNA insertion mutants from *Arabidopsis thaliana*.

**Supplemental Figure S6.** CRISPR/Cas9 strategy to obtain deletion mutants.

**Supplemental Table S1.** UniProt accession numbers of the proteins used for the phylogenetic study.

**Supplemental Table S2.** Primers used in this study.

### Acknowledgments

We would like to thank Tiphaine Dhalleine (Univ. Lorraine) for the help with the purifications of mFDX-like proteins and Michael Tillich for the help in designing the guide RNAs.

### Funding

The work was financially supported by a grant of the Deutsche Forschungsgemeinschaft (ME 4174/3-1) to E.H.M; by the Kempe Foundations (Gunnar Öquist Fellowship)

and T4F to O.K; by KSLA to J.P.T; by a funding from the Lorraine University of Excellence (LUE) to N.R.

*Conflict of interest statement.* None declared.

## References

- Baradaran R, Berrisford JM, Minhas GS, Sazanov LA** (2013) Crystal structure of the entire respiratory complex I. *Nature* **494**(7438): 443–448
- Bellido AM, Distefano AM, Setzes N, Cascallares MM, Oklestkova J, Novak O, Ramirez JA, Zabaleta EJ, Fiol DF, Pagnussat GC** (2022) A mitochondrial ADXR-ADX-P450 electron transport chain is essential for maternal gametophytic control of embryogenesis in *Arabidopsis*. *Proc Natl Acad Sci U S A* **119**(4): e2000482119
- Blake JA, Lee KW, Morris TJ, Elthon TE** (2007) Effects of turnip crinkle virus infection on the structure and function of mitochondria and expression of stress proteins in turnips. *Physiol Plant* **129**(4): 698–706
- Braun HP** (2020) The oxidative phosphorylation system of the mitochondria in plants. *Mitochondrion* **53**: 66–75
- Braun HP, Binder S, Brennicke A, Eubel H, Fernie AR, Finkemeier I, Klodmann J, König AC, Kühn K, Meyer E, et al.** (2014) The life of plant mitochondrial complex I. *Mitochondrion* **19 Pt B**: 295–313
- Cainzos M, Marchetti F, Popovich C, Leonardi P, Pagnussat G, Zabaleta E** (2021) Gamma carbonic anhydrases are subunits of the mitochondrial complex I of diatoms. *Mol Microbiol* **116**(1): 109–125
- Cardol P** (2011) Mitochondrial NADH:ubiquinone oxidoreductase (complex I) in eukaryotes: a highly conserved subunit composition highlighted by mining of protein databases. *Biochim Biophys Acta* **1807**(11): 1390–1397
- Cardol P, Vanrobaeys F, Devreese B, Van Beeumen J, Matagne RF, Remacle C** (2004) Higher plant-like subunit composition of mitochondrial complex I from *Chlamydomonas reinhardtii*: 31 conserved components among eukaryotes. *Biochim Biophys Acta* **1658**(3): 212–224
- Carrie C, Giraud E, Duncan O, Xu L, Wang Y, Huang S, Clifton R, Murcha M, Filipovska A, Rackham O, et al.** (2010) Conserved and novel functions for *Arabidopsis thaliana* MIA40 in assembly of proteins in mitochondria and peroxisomes. *J Biol Chem* **285**(46): 36138–36148
- Carrie C, Kuhn K, Murcha MW, Duncan O, Small ID, O’Toole N, Whelan J** (2009) Approaches to defining dual-targeted proteins in *Arabidopsis*. *Plant J* **57**(6): 1128–1139
- Clark KA, Krysan PJ** (2010) Chromosomal translocations are a common phenomenon in *Arabidopsis thaliana* T-DNA insertion lines. *Plant J* **64**(6): 990–1001
- Davies KM, Blum TB, Kuhlbrandt W** (2018) Conserved in situ arrangement of complex I and III2 in mitochondrial respiratory chain supercomplexes of mammals, yeast, and plants. *Proc Natl Acad Sci U S A* **115**(12): 3024–3029
- Efremov RG, Sazanov LA** (2012) The coupling mechanism of respiratory complex I—a structural and evolutionary perspective. *Biochim Biophys Acta* **1817**(10): 1785–1795
- Enriquez JA** (2016) Supramolecular organization of respiratory complexes. *Annu Rev Physiol* **78**(1): 533–561
- Eubel H, Braun HP, Millar AH** (2005) Blue-native PAGE in plants: a tool in analysis of protein-protein interactions. *Plant Methods* **1**(1): 11
- Fromm S, Braun HP, Peterhansel C** (2016) Mitochondrial gamma carbonic anhydrases are required for complex I assembly and plant reproductive development. *New Phytologist* **211**(1): 194–207
- Fuchs P, Rugen N, Carrie C, Elsasser M, Finkemeier I, Giese J, Hildebrandt TM, Kuhn K, Maurino VG, Ruberti C, et al.** (2020) Single organelle function and organization as estimated from *Arabidopsis* mitochondrial proteomics. *Plant J* **101**(2): 420–441
- Gu J, Wu M, Guo R, Yan K, Lei J, Gao N, Yang M** (2016) The architecture of the mammalian respirasome. *Nature* **537**(7622): 639–643
- Gutierrez S, Sabar M, Lelandais C, Chetrit P, Diolez P, Degand H, Boutry M, Vedel F, De Kouchkovsky Y, De Paepe R** (1997) Lack of mitochondrial and nuclear-encoded subunits of complex I and alteration of the respiratory chain in *Nicotiana glauca* mitochondrial deletion mutants. *Proc Natl Acad Sci U S A* **94**(7): 3436–3441
- Hanke G, Mulo P** (2013) Plant type ferredoxins and ferredoxin-dependent metabolism. *Plant Cell Environ* **36**(6): 1071–1084
- Hansen BO, Meyer EH, Ferrari C, Vaid N, Movahedi S, Vandepoele K, Nikoloski Z, Mutwil M** (2018) Ensemble gene function prediction database reveals genes important for complex I formation in *Arabidopsis thaliana*. *New Phytol* **217**(4): 1521–1534
- Heazlewood JL, Tonti-Filippini JS, Gout AM, Day DA, Whelan J, Millar AH** (2004) Experimental analysis of the *Arabidopsis* mitochondrial proteome highlights signaling and regulatory components, provides assessment of targeting prediction programs, and indicates plant-specific mitochondrial proteins. *Plant Cell* **16**(1): 241–256
- Hirst J** (2013) Mitochondrial complex I. *Annu Rev Biochem* **82**(1): 551–575
- Hirst J** (2018) Open questions: respiratory chain supercomplexes—why are they there and what do they do? *BMC Biol* **16**(1): 111
- Javadov S, Jang S, Chapa-Dubocq XR, Khuchua Z, Camara AK** (2021) Mitochondrial respiratory supercomplexes in mammalian cells: structural versus functional role. *J Mol Med (Berl)* **99**(1): 57–73
- Kampjut D, Sazanov LA** (2020) The coupling mechanism of mammalian respiratory complex I. *Science* **370**(6516): 172–182
- Klusck N, Dreimann M, Senkler J, Rugen N, Kuhlbrandt W, Braun HP** (2023) Cryo-EM structure of the respiratory I + III(2) supercomplex from *Arabidopsis thaliana* at 2 Å resolution. *Nat Plants* **9**: 142–156
- Klusck N, Senkler J, Yildiz O, Kuhlbrandt W, Braun HP** (2021) A ferredoxin bridge connects the two arms of plant mitochondrial complex I. *Plant Cell* **33**(6): 2072–2091
- Kolata P, Efremov RG** (2021) Structure of *Escherichia coli* respiratory complex I reconstituted into lipid nanodiscs reveals an uncoupled conformation. *Elife* **10**: e68710
- Koprivova A, Des Francs-Small CC, Calder G, Mugford ST, Tanz S, Lee BR, Zechmann B, Small I, Kopriva S** (2010) Identification of a pentatricopeptide repeat protein implicated in splicing of intron 1 of mitochondrial *nad7* transcripts. *J Biol Chem* **285**(42): 32192–9
- Kühn K, Obata T, Feher K, Bock R, Fernie AR, Meyer EH** (2015) Complete mitochondrial complex I deficiency induces an upregulation of respiratory fluxes that is abolished by traces of functional complex I. *Plant Physiol* **168**(4): 1537–1549
- Lampropoulos A, Sutikovic Z, Wenzl C, Maegele I, Lohmann JU, Forner J** (2013) Greengate—a novel, versatile, and efficient cloning system for plant transgenesis. *PLoS One* **8**(12): e83043
- Lenaz G, Genova ML** (2009) Structural and functional organization of the mitochondrial respiratory chain: a dynamic super-assembly. *Int J Biochem Cell Biol* **41**(10): 1750–1772
- Letts JA, Fiedorczuk K, Degliesposti G, Skehel M, Sazanov LA** (2019) Structures of respiratory supercomplex I + III2 reveal functional and conformational crosstalk. *Mol Cell* **75**(6): 1131–1146 e6
- Letts JA, Sazanov LA** (2015) Gaining mass: the structure of respiratory complex I from bacterial towards mitochondrial versions. *Curr Opin Struct Biol* **33**: 135–145
- Ligas J, Pineau E, Bock R, Huynen MA, Meyer EH** (2019) The assembly pathway of complex I in *Arabidopsis thaliana*. *Plant J* **97**(3): 447–459
- Lopez-Lopez A, Keech O, Rouhier N** (2022) Maturation and assembly of iron-sulfur cluster-containing subunits in the mitochondrial Complex I from plants. *Front Plant Sci* **13**: 916948
- Maldonado M, Fan Z, Abe KM, Letts JA** (2023) Plant-specific features of respiratory supercomplex I + III(2) from *Vigna radiata*. *Nat Plants* **9**: 157–168
- Maldonado M, Padavannil A, Zhou L, Guo F, Letts JA** (2020) Atomic structure of a mitochondrial complex I intermediate from vascular plants. *Elife* **9**: e56664

- Meyer EH, Letts JA, Maldonado M** (2022) Structural insights into the assembly and the function of the plant oxidative phosphorylation system. *New Phytol* **235**(4): 1315–1329
- Meyer EH, Solheim C, Tanz SK, Bonnard G, Millar AH** (2011) Insights into the composition and assembly of the membrane arm of plant complex I through analysis of subcomplexes in Arabidopsis mutant lines. *J Biol Chem* **286**(29): 26081–26092
- Meyer EH, Tomaz T, Carroll AJ, Estavillo G, Delannoy E, Tanz SK, Small ID, Pogson BJ, Millar AH** (2009) Remodeled respiration in *ndufs4* with low phosphorylation efficiency suppresses Arabidopsis germination and growth and alters control of metabolism at night. *Plant Physiol* **151**(2): 603–619
- Michaud M, Gros V, Tardif M, Brugiere S, Ferro M, Prinz WA, Toulmay A, Mathur J, Wozny M, Falconet D, et al.** (2016) Atmic60 is involved in plant mitochondria lipid trafficking and is part of a large complex. *Curr Biol* **26**(5): 627–639
- Milenkovic D, Blaza JN, Larsson NG, Hirst J** (2017) The Enigma of the respiratory chain supercomplex. *Cell Metab* **25**(4): 765–776
- Nicholls DG, Ferguson SJ** (2013) *Bioenergetics*. Academic Press, Elsevier, Amsterdam
- Niehaus M, Straube H, Kunzler P, Rugen N, Hegermann J, Giavalisco P, Eubel H, Witte CP, Herde M** (2020) Rapid affinity purification of tagged plant mitochondria (mito-AP) for metabolome and proteome analyses. *Plant Physiol* **182**(3): 1194–1210
- Parey K, Lasham J, Mills DJ, Djurabekova A, Haapanen O, Yoga EG, Xie H, Kuhlbrandt W, Sharma V, Vonck J, et al.** (2021) High-resolution structure and dynamics of mitochondrial complex I—insights into the proton pumping mechanism. *Sci Adv* **7**(46): eabj3221
- Perales M, Eubel H, Heinemeyer J, Colaneri A, Zabaleta E, Braun HP** (2005) Disruption of a nuclear gene encoding a mitochondrial gamma carbonic anhydrase reduces complex I and supercomplex I + III2 levels and alters mitochondrial physiology in Arabidopsis. *J Mol Biol* **350**(2): 263–277
- Peters K, Belt K, Braun HP** (2013) 3D Gel map of Arabidopsis complex I. *Front Plant Sci* **4**: 153
- Peterson R, Slovin JP, Chen C** (2010) A simplified method for differential staining of aborted and non-aborted pollen grains. *Int J Plant Biol* **1**(2): e13
- Picciochi A, Douce R, Alban C** (2003) The plant biotin synthase reaction. Identification and characterization of essential mitochondrial accessory protein components. *J Biol Chem* **278**(27): 24966–24975
- Przybyla-Toscano J, Christ L, Keech O, Rouhier N** (2021) Iron-sulfur proteins in plant mitochondria: roles and maturation. *J Exp Bot* **72**(6): 2014–2044
- Przybyla-Toscano J, Roland M, Gaymard F, Couturier J, Rouhier N** (2018) Roles and maturation of iron-sulfur proteins in plastids. *J Biol Inorg Chem* **23**(4): 545–566
- Pucker B, Kleinbolting N, Weishaar B** (2021) Large scale genomic rearrangements in selected Arabidopsis thaliana T-DNA lines are caused by T-DNA insertion mutagenesis. *BMC Genomics* **22**(1): 599
- Ruf S, Forner J, Hasse C, Kroop X, Seeger S, Schollbach L, Schadach A, Bock R** (2019) High-efficiency generation of fertile transplastomic Arabidopsis plants. *Nat Plants* **5**(3): 282–289
- Sabar M, Balk J, Leaver CJ** (2005) Histochemical staining and quantification of plant mitochondrial respiratory chain complexes using blue-native polyacrylamide gel electrophoresis. *Plant J* **44**(5): 893–901
- Schagger H, Pfeiffer K** (2001) The ratio of oxidative phosphorylation complexes I–V in bovine heart mitochondria and the composition of respiratory chain supercomplexes. *J Biol Chem* **276**(41): 37861–7
- Schagger H, Von Jagow G** (1991) Blue native electrophoresis for isolation of membrane protein complexes in enzymatically active form. *Anal Biochem* **199**(2): 223–231
- Schertl P, Sunderhaus S, Klodmann J, Grozeff GE, Bartoli CG, Braun HP** (2012) L-galactono-1,4-lactone dehydrogenase (GLDH) forms part of three subcomplexes of mitochondrial complex I in Arabidopsis thaliana. *J Biol Chem* **287**(18): 14412–9
- Schimmeyer J, Bock R, Meyer EH** (2016) L-Galactono-1,4-lactone dehydrogenase is an assembly factor of the membrane arm of mitochondrial complex I in Arabidopsis. *Plant Mol Biol* **90**(1–2): 117–126
- Senkler J, Senkler M, Eubel H, Hildebrandt T, Lengwenus C, Schertl P, Schwarzlander M, Wagner S, Wittig I, Braun HP** (2017) The mitochondrial complexome of Arabidopsis thaliana. *Plant J* **89**(6): 1079–1092
- Soufari H, Parrot C, Kuhn L, Waltz F, Hashem Y** (2020) Specific features and assembly of the plant mitochondrial complex I revealed by cryo-EM. *Nat Commun* **11**(1): 5195
- Stuchebrukhov A, Schafer J, Berg J, Brzezinski P** (2020) Kinetic advantage of forming respiratory supercomplexes. *Biochim Biophys Acta Bioenerg* **1861**(7): 148193
- Sunderhaus S, Dudkina NV, Jansch L, Klodmann J, Heinemeyer J, Perales M, Zabaleta E, Boekema EJ, Braun HP** (2006) Carbonic anhydrase subunits form a matrix-exposed domain attached to the membrane arm of mitochondrial complex I in plants. *J Biol Chem* **281**(10): 6482–6488
- Takubo K, Morikawa T, Nonaka Y, Mizutani M, Takenaka S, Takabe K, Takahashi MA, Ohta D** (2003) Identification and molecular characterization of mitochondrial ferredoxins and ferredoxin reductase from Arabidopsis. *Plant Mol Biol* **52**(4): 817–830
- Tamura K, Stecher G, Kumar S** (2021) MEGA11: molecular evolutionary genetics analysis version 11. *Mol Biol Evol* **38**(7): 3022–3027
- Wang ZP, Xing HL, Dong L, Zhang HY, Han CY, Wang XC, Chen QJ** (2015) Egg cell-specific promoter-controlled CRISPR/Cas9 efficiently generates homozygous mutants for multiple target genes in Arabidopsis in a single generation. *Genome Biol* **16**(1): 144
- Wu M, Gu J, Zong S, Guo R, Liu T, Yang M** (2020) Research journey of respirasome. *Protein Cell* **11**(5): 318–338
- Zhou L, Maldonado M, Padavannil A, Guo F, Letts JA** (2022) Structures of Tetrahymena's Respiratory chain reveal the diversity of eukaryotic core metabolism. *Science* **376**(6595): 831–839